Click here to view linked References

Structure and microstructure evolution of Al–Mg–Si alloy processed by equal channel angular pressing

T. Khelfa[1*], M. A. Rekik[1], M. Khitouni[1], J. M. Cabrera-Marrero[2,3]

[1] Laboratory of Inorganic chemistry Ur-11-ES-73, Faculty of Sciences, University of Sfax, 1171, 3018-Sfax, Tunisia.
[2] Department of Materials Science and Metallurgical Engineering Universitat Politècnica de Catalunya ETSEIB-Av. Diagonal 647, 08028 – Barcelona, Spain
[3] Fundación CTM Centro Tecnológico, Plaza de la Ciencia 2, 08243-Manresa, Spain

Abstract

An ultrafine grained Al–Mg–Si alloy was prepared by severe plastic deformation using the Equal Channel Angular Pressing (ECAP) method. Samples were ECAPed through a die with an inner angle of $\Phi=90º$ and outer arc of curvature of $\psi= 37°$ from 1 to 12 ECAP passes at room temperature following route B_c. To analyze the evolution of the microstructure at increasing ECAP passes x-ray diffraction and Electron Backscatter Diffraction analyses were carried out. The results revealed two distinct processing regimes, namely: i) from 1 to 5 passes, the microstructure evolved from elongated grains and sub-grains to a rather equiaxed array of ultrafine grains and ii) from 5 to 12 passes where no change in the morphology and average grain size was noticed. In the overall behavior, the boundary misorientation angle and the fraction of high-angle boundaries increase rapidly up to 5 passes and at a lower rate from 5 to 12 passes. The crystallite size decreased down to about 45 nm with the increase in deformation. The influence of deformation on precipitate evolution in the Al–Mg–Si alloy was also studied by differential scanning calorimetry. A significant decrease in the peak temperature associated to the 50% of recrystallization was observed at increasing ECAP passes.

Keywords: Equal-channel angular pressing (ECAP); aluminum alloy; X-ray diffraction (XRD); Microstructure; Differential scanning calorimetry (DSC).

*Corresponding author: tarekkhelfa@yahoo.fr

1. Introduction

In recent years, great attention of researchers has been drawn to ultrafine-grained (UFG) metallic materials in which the structure refinement is achieved by severe plastic deformation (SPD) [1–3]. One of the SPD methods having a promising potential for industrial applications is the so-called Equal Channel Angular Pressing (ECAP) [4]. During ECAP, a sample in the form of a rod or bar is pressed through a die formed by two channels of equal cross section intersecting internally at an angle Φ, which usually ranges between 60 and 160º. There is also an additional angle Ψ that defines the curvature arc at the outer point of intersection of the two channels. Among the most important incentives for using this technique is that the cross-section sample remains unchanged during processing.

Al–Mg–Si alloys represent an important group of materials often used as structural material for construction and transportation applications thanks to their excellent corrosion resistance, weldability, extrudability and response to surface finishing operations. The ECAP process is believed to provide a useful tool to make strong Al-Mg-Si alloys through microstructural refinement. It is feasible to repeat the pressing several times to achieve a large degree of strain and thereby, to refine the grain size to a submicrometer or even nanometer level. The nanostructured materials produced by ECAP have a very high strength due to their low grain size (and therefore large number of grain boundaries) and high amount of defects, such as vacancies, dislocations and staking faults [5-9]. Because most structural transformations and mechanical properties are associated with the vacancies, dislocations, stacking faults and grain boundaries, a precise quantification of such defects in ultrafine grains alloys seems necessary for better understanding and control of the final properties. The microstructural features such as the lattice parameter, the average crystallite size, the lattice strains, the dislocation density and the phase proportion can be obtained from detailed analyses of the X-ray diffraction (XRD) profiles using the Rietveld refinement and the

Warren-Averbach, the Williamson-Hall and the Halder-Wagner methods. In the present work, the analysis of the XRD profiles was performed via the Halder–Wagner (HW) method. Most of these methods evaluate the influence of grain size and strain on the shape of the diffraction peaks [10].

Regarding ECAP processing, many research works have already commonly pointed out that during the first passes the microstructure consists of parallel subgrains bands which subsequently evolve with further pressing into an array of grains separated by high angle grain boundaries (HAGBs) [11, 12]. On the other hand, among the age hardenable aluminum alloys, the Al–Mg–Si system has been the object of extensive investigation considering its technological importance as the basis of the high strength aluminum alloys. The precipitation sequence usually proposed for this type of alloys is as follows [13, 14]:

Supersaturated solid solution $\alpha_{sss} \rightarrow$ spherical Guinier-Preston (GP) zones $\rightarrow \beta''$ precipitates $\rightarrow \beta'$ precipitates $\rightarrow \beta$ precipitates

The supersaturated solid solution (α_{sss}) is obtained by a solid solution treatment. The decomposition starts with the formation and growth of GP-zones (generally spherical clusters), meanwhile the pre-aging treatment. β'' precipitates are fine needle-shaped zones with monoclinic structure and are found in Al alloys aged to the maximum hardness; β' particles are rod-shaped precipitates with hexagonal structure and are present in overaged specimens, and finally β (Mg_2Si) is the equilibrium phase in the precipitation sequence.

Several researches works have shown that both the precipitation kinetics and sequence mainly change when the alloy structure is deformed plastically. As the density of defects increase, the precipitation temperatures of some phases decrease. Consequently, this behavior can lead to the anticipation of the metastable β''/ β' peak temperature, the creation of obvious peak of the GP zones and finally the reduction of Mg_2Si and Si amount ratio in the eventually formed phases. Farè et al. [15] and Vedani et al. [16] have reported that the precipitation

3

kinetics in Al-Mg-Si alloys depend on the strain accumulated during the ECAP process. They noticed that the diffraction peak positions and activation energies were a function of the ECAP passes, and explained how the precipitation kinetics in ultra fine grained (UFG) alloys was largely affected regarding the coarse-grained materials.

The aim of the present paper is to process an Al–Mg-Si alloy (AA6060) by ECAP at room temperature and provide an interpretation of the results through structural and microstructural investigation using XRD and EBSD analyses. Furthermore, the DSC technique was used to understand the evolution of precipitation behavior of the deformed samples of AA6060 and draw conclusions on their dependence on the ECAP process.

2. Experimental procedure

The experiments were conducted using an Al–Mg-Si alloy (AA6060) in the artificially aged condition T6. Table 1 presents the chemical composition of the AA6060 used in this study. The alloy was received in the form of extruded bar, and then machined into cylindrical specimens of 60 mm in length and 10 mm in diameter. The ECAP process was carried out at room temperature through a solid die fabricated from a tool steel with a channel angle of $\Phi = 90º$ and a curvature angle of $\psi = 37°$ (Fig. 1) using a pressing speed of 0.02 m/s. Molybdenum disulfide (MoS_2) was used as lubricant. Samples were pressed from 1 to 12 passes via route B_c, i.e. the sample was rotated along the longitudinal axis by 90° in the same direction after each pass. This route is recognized to lead even most rapidly to a homogeneous microstructure of equiaxed grains. As already known, the total strain developed during ECAP is given by Iwahashi et al.'s equation (1) [17]:

$$\varepsilon_N = \frac{N}{\sqrt{3}} \left[2\cot\left\{ \left(\frac{\Phi}{2}\right) + \left(\frac{\psi}{2}\right) \right\} + \psi\,\text{cosec}\left\{ \left(\frac{\Phi}{2}\right) + \left(\frac{\psi}{2}\right) \right\} \right] \tag{1}$$

where ε_N is the strain after N cycles, Φ and Ψ are the die corner angle and the die angle, respectively. According to equation (1), the geometric configuration presented in Fig. 1 produced a strain of $\varepsilon \sim 1$ in each pass.

4

The x-ray diffraction measurements of the ECAPed Al-Mg-Si samples were carried out on a Philips X pert Pro diffractometer with a Cu-K_α radiation between 30° and 90° using 0.017° per 4 s step size. The instrumental broadening was determined from the measurement of an Si standard. The crystallite size <D> and the equivalent lattice strain $<\varepsilon^2>^{1/2}$ were determined from the peak broadening (β) using the Halder-Wagner (HW) approach [18] based on the slope and the ordinate intersection of the line plotted according to the following equation (2):

$$(\beta^*/d^*)^2 = D^{-1}\beta^*/(d^*)^2 + (\varepsilon/2)^2 \qquad (2)$$

where $\beta^* = \beta\cos\theta/\lambda$ and $d^* = 2\sin\theta/\lambda$; θ is the Bragg angle and λ is the wavelength used.

The lattice parameter before and after ECAP was extracted from a linear regression analysis, a_{hkl} deduced from each peak, and plotted using the Nilson–Reley (NR) function given by the below equation (3) [19]:

$$N\text{-}R = (\cos2\theta/\sin\theta + \cos2\theta/\theta)/2 \qquad (3)$$

and extrapolated to NR = 0, that is 2θ = 180°.

The microstructures of the deformed samples were characterized by EBSD on the transversal plane (XY plane). For this purpose, the samples were cut from the center of the ECAP samples and mechanically polished with 2500 grit SiC paper until 0.02 μm colloidal silica suspension followed by electropolishing in a 100 ml $HClO_4$+900 ml C_2H_5OH solution at -20 °C and a voltage of 20 V.

Aiming to clarify the precipitation sequence and the peak temperatures, the miniature specimens of 20−35 mg were cut near the axial centre of the as-pressed samples and subjected to DSC analysis using a Labsys Evo (1600 °C) facility at a constant heating rate of 20 °C/min under argon atmosphere and in a temperature range from 30 to 500 °C. Each sample was placed in an Al_2O_3 crucible and introduced into the DSC furnace, while an empty Al_2O_3 crucible was used as reference.

3. Results and discussion

3.1. X-ray diffraction analysis

Figure 2 depicts the XRD patterns of the analyzed specimens before and after ECAP process. As shown in the XRD pattern of the undeformed sample, the (111), (200), (220), (311) and (222) fundamental reflections were recorded for the fcc-Al structure. In addition, two supplementary peaks at $2\theta=47.88°$ and $48.62°$ of lower intensities were identified to be characteristic of the Al_8Fe_2Si fine precipitates with hexagonal structure [20, 21]. Besides, one can observe the presence of undissolved Cu-rich (Al-Cu-Mg-Si) and Fe-rich (Al-Fe-Si) phases. Next, Mg_2Si precipitates can be identified by a reflexion at $2\theta = 40.21°$ [22]. However, the presence of Mg_2Si peak is not observed in all ECAPed samples. Indeed, after the first pass, Mg_2Si and Al_8Fe_2Si precipitates dissolved, due to the induced heavy strain, whereas the iron rich phase is still observed. Nevertheless, a small Mg_2Si peak is still observed after four passes. Panigrahi et al. [23] reported that the formation of the Mg_2Si phase after SPD could be explained by the accumulation of dislocations that may act as a short-circuit path for solutes and atomic migration facilitating this precipitation. Furthermore, they added that the frictional heat induced on the sample caused a clustering of Mg and Si atoms with vacancies, leading to the formation of Mg_2Si peak in the XRD pattern. The Cu-rich phase, in turn, was totally dissolved inside the Al matrix due to the induced strain in the ECAPed samples after the first five passes. After that, this phase was observed to be precipitated until 12 passes. On the other hand, the observed Bragg reflections were broadened after the ECAP process, which is related to the reduction of crystallite size and to the important lattice strain introduced by ECAP. Figure 3 shows typical broadening of the most intense $(111)_{Al}$ and $(200)_{Al}$ reflections with ECAP passes number. The variations of the crystallite size <D> and the lattice strain (ε) were determined from the XRD reflections profiles using the HW method (Fig. 4), and results are displayed in Fig. 5. An obvious

6

intensive grain refinement is clearly noticed after the ECAP process. In fact, the crystallite size already reached ∼ 45 nm after the first ECAP pass accompanied by a substantial increase of ε which can be related to the high amount of deformation introduced. From 2 to 6 passes, no systematic variation is observed and the average values for crystallite size and lattice strains are about 52 nm and 0.23 %, respectively. Both curves have up-down variations of these parameters that could be related to the characteristic of the processing mechanics of the route Bc as well as the fact that SPD may lead to several modifications such as dislocation activities, vacancies, and atomic site interchange [24]. On the other hand, Reyes et al. [25] have shown a maximum of the lattice strain between passes 2 and 3 in the case of AA6061-T6, and then remained steady after 5 passes. They interpreted this behavior by the optimum number of ECAP passes to achieve a stable configuration of dislocations. This behavior is quite similar with that obtained in the present results. It is of quite importance to mention that the average crystallite size after 12 passes is very similar to the one at 4th and subsequent passes, indicating that the crystallite size remains approximately constant after four passes.

The lattice strain and theoretical strain induced during ECAP are plotted against the number of passes and given in Fig. 6. There is a large variation in lattice strain when compared to the theoretical one during ECAP. The above anomalous behavior can be explained by the high amount of severe plastic deformation introduced by ECAP, which enhances the grains boundaries (GBs) mobility and leads to the increase of the crystallite size. Increasing the number of passes up to five, the lattice strain decreases, which may be attributed to dynamic recovery activation. For a larger number of passes (up to 12 passes), lattice strain achieves a saturation value, which can be explained in terms of a balance between work hardening and softening by dynamic recovery.

The examination of the diffraction patterns obtained after ECAP processing shows that peaks are shifted to high θ values (Fig. 3). Such behavior has been explained in the literature

by the creation of stacking faults by intensive deformation and variation of the lattice parameter during ECAP. The evolution of the lattice parameter against ECAP passes number is given in Fig. 7. After the three first passes, one can clearly notice an important decrease in the lattice parameter. The maximum variation was ~ -0.1% for the third ECAP pass, and thereafter, it slightly increased. However, it remained lower than that of the unpressed AA6060. Moreover, the obtained values are much higher than the lattice parameter for pure aluminum (a=4.0494 Å) [26]. This fact can testify the retention of a large quantity of Si and Mg atoms in the aluminum lattice after artificial aging. The decrease of the lattice parameter was probably due to the ECAP strain or to the partial precipitates dissolution due to the role of Si and Fe in decrease the lattice parameter in aluminum matrix [27, 28]. In addition, it has been shown that a reduction of grain size can also explain the decrease of lattice parameter [29, 30]. The slight increase of the lattice parameter up to 4 passes is followed by a decrease after 5 passes. After that, a steady state step of variation for extended ECAP passes until 12 passes was noted. In conclusion, the lattice parameter did not change regularly during ECAP process. This behaviour of the cell parameter as a function of the number of passes arises mainly from two opposing alloying effects [31, 32]: i) the existence of vacancies and dissolution of the elements, having lower atomic radii (e.g. Fe (1.17 Å) and Si (1.26 Å)) than Al (1.43 Å) decrease the lattice parameter and ii) the dissolution of elements, having higher atomic radii (e.g. Mg (1.6 Å) element) than Al element, increases the lattice parameter. Besides, the total solubility of precipitate increases the lattice parameter [31].

Figure 8 shows the variation of the dislocation density (ρ) as a function of ECAP pass number. For severe plastic deformed samples, dislocation density, ρ, can be calculated in terms of the crystallite size, $<D>$, the root-square lattice strains, $<\varepsilon^2>^{1/2}$, and the Burger's vector, b, according to equation (4) [33]:

8

$$\rho_D = 2\sqrt{3}\frac{<\varepsilon^2>^{1/2}}{<D>\times b} \qquad (4)$$

where b equal to a $\frac{\sqrt{2}}{2}$ for the FCC structure, being a the lattice parameter.

It is clearly seen that ρ_D increases from about 0.01×10^{15} m^{-2} to 1.29×10^{15} m^{-2} the increase in ECAP from 0 to 2 passes, and then slightly decreases to about 1×10^{15} m^{-2} after five passes and the remains unchanged at a steady-state value. This decrease can be explained by partial dynamic recrystallization. Generally, in conventional polycrystalline materials, the GBs are thought to be barriers to the dislocations motion. Therefore, the slight decrease in the dislocations density within further ECAP passes indicates a softening of the GBs. When the GBs have become soft or relaxed, the level of the dislocations piled up near the GBs will decrease [24, 25]. The steady state value of dislocation can be explained by the structure refinement of the ECAP samples, in which the small crystallites become, themselves, a limit for the dislocation glide and, consequently, for further ECAP pressing, the level of dislocation density remains unchanged.

3.2. Microstructure

Figure 9 illustrates the AA6060 microstructural attitude, before and after ECAP process. The black and white lines from the EBSD maps indicate the location of high angle grain boundaries (HAGB) ($\theta \geq 15°$) and low angle grain boundaries (LAGB) ($3°\leq \theta \leq 15°$), respectively. The microstructure of the as-received material exhibits equiaxed grain morphology with an average grain size of ~52 µm (Fig. 9a). The morphology and the microstructure becomes elongated after the first ECAP pass (Fig. 9b), and the obtained average grain size is around 1.33 µm with a well-enhanced subgrain microstructure. As shown in Fig. 9(c-d), after two and three passes, the microstructure has apparently the same appearance as the banded structure after 1 pass. The widths of the bands in this condition were measured to give an average size of 1µm. After the fourth ECAP pass, it is obvious that the

sub-grains within the coarse grains are generally either equiaxed or elongated with an average grain size of 0.68μm (Fig. 9e). After five, six and eight passes (Fig. 9(f-h)), a significant increase in the number of HAGB was revealed and the average grain sizes of 0.51, 0.52 and 0.57 μm were obtained, respectively. Finally after twelve passes of ECAP, the microstructure consists of elongated grains together with smaller and equiaxed grains of 0.47μm (Fig. 9i).

The distribution of the grain boundary misorientations is shown in Fig. 10 for the samples processed through 1, 2, 4, 5, 8 and 12 passes, respectively. After 1 pass of ECAP, there is a very large number of LAGB representing 69.8% of all boundaries in the sample (Fig. 10a). However, the fraction of HAGB increases with the increase in processing by ECAP reaching ~56 % after 5 passes (Fig. 10d) and ~61% after 12 passes (Fig. 10f). The relatively slow evolution to HGAB in the AA6060 can be related to the presence of solute atoms that impede HAGB dislocation movement and lead to a slower rate of recovery [34]. In the case of high purity Al processed by ECAP, Kawasaki et al. [35] have reported that the fraction of HAGB increases from 53 % after 8 passes to 74 % after 12 ECAP passes. Moreover, (Fig. 9(e,f)) show that small peaks appear in the high angle region (50-60º), which suggests that more LAGB have transformed into HAGB with the increase of the number of ECAP passes.

Figure 11 depicts the dependence of the average grain size as function of the ECAP passes number. As already mentioned, the initial grain size of the undeformed sample was ~52 μm. It is apparent that the grain size decreases rapidly to ~ 1.33 μm after a single pass. Subsequently, the results show a very sharp decrease in the grain size to ~ 0.5 μm after 5 passes. Nevertheless, the grain size remains essentially constant up to 12 ECAP passes (Fig. 11a). This behavior was very similar to that found in Kim et al. [36] results for an ECAPed AA6061 alloy at room temperature. Kawasaki et al. [35] have concluded that for ECAPed pure Al, there is no additional grain refinement with the increase in the number of passes

(~1.3 μm). Yet, Iwahashi et al. [37] have stated the addition of magnesium, as an alloying element, to an aluminum matrix decreases the grain size from 0.45 μm for Al-1%Mg (after 6 passes) and ~0.27 μm for Al-3%Mg (after 8 passes). The occurrence of smaller grain sizes when alloying with magnesium is attributed to the decreasing rates of recovery in these solid solution alloys [37]. Concerning to the grain boundaries nature (Fig. 11b), it clearly seen that the processed material has a wide quantity of subgrains formed in the first pass, which decreases progressively with the increase of ECAP passes. In the initial stage of SPD processing, the necessary geometrical boundaries are formed to subdivide the coarse grains into cell blocks [38]. For that reason, in the first ECAP pass, a high fraction of LAGB was found, while in the following passes HAGB increases continuously. After 12 ECAP passes, the value of ~0.61 noted for the fraction of high-angle misorientations is similar to that found in an earlier report for Al–Mg alloy (~0.57) processed through 12 ECAP passes [34]. In fact, the proportion of HAGB after 12 passes is found to be similar to that of the undeformed material. .

3.3. DSC analyses

Figure 12 presents the recorded DSC runs of the Al–Mg–Si alloy as a function of ECAP passes number. The DSC curve for the undeformed sample shows three exothermic peaks (noted 1, 2 and 3) and one endothermic peak (noted 2'). As regards, the exothermic reaction peak 1 occurred from 185 to 230 °C and represents the formation of solute rich clusters. With respect to the broad exothermic peak 2 at about 325 °C, it can be attributed to the β'' precipitation. It has been reported that a second peak, usually located at about 330 °C and corresponding to β' formation, might be superimposed to a shoulder of the former peak or even completely hidden by it [39]. More precisely, it has been mentioned that the sub-peak at 325 °C is probably related to the Si-rich particles precipitation which act as motifs to form of the β'' phase and the noticeable peak at 330 °C refers to the creation of both rod-shaped β'-

11

phase and large Si-rich precipitates [40,41]. A broad dissolution endothermic peak 2' of the above phases appear at temperature range of 375-420 °C, whereas the third marked exothermic peak at 445 °C due to the creation of β-Mg_2Si equilibrium phase. The ECAP processed alloy shows remarkable differences in the peaks position and shape. After the first ECAP pass, a new exothermic peak is observed at a temperature range of 240–270 °C following an endothermic peak in the range of 275–285 °C. This may be attributed to the formation and the dissolution of the preformed clusters/GP zones, respectively. Additionally, the above described broad peak attributed to the formation of β'' and β' phases appears now as a broader peak centered at 375 °C. Hence the broadening peak might be the result of the overlap between β' peak and β peak, following an endothermic peak at around 475 °C related to the dissolution of the β-Mg_2Si equilibrium phase. Furthermore, the careful observations of the curves corresponding to passes 2 to 12 of the ECAP processed samples suggest that heavy plastic deformation has separated the two originally superimposed peaks of β'' and β' phases. Stable β precipitates formed in the deformed alloy has shown to be notably anticipated (390–425 °C) and of continuously reduced intensity regarding the undeformed sample. It is also interesting to note that the peak of β' precipitates after eight ECAP passes is reduced. According to Matsuda et al. [42] the reduction of the β' precipitates in alloys with the excess of Si, resulted from the creation of Si-rich metastable phases (type-B and type-A) as a competing phase to β'.Then, the possible depletion in Si from the matrix could also reduce the formation of β-Mg_2Si stable phase. When comparing the curve of the first ECAP pass to that of the other ECAP processed samples, it is evident that significant modifications occurred due to the severe plastic deformation experienced by the alloy. There is clear evidence that the broad peak at 375 °C is shifted to lower temperatures in the ECAP processed samples. The position of this β' peak is shown in Fig. 13 as a function of the number ECAP passes. This peak temperature moves from 386 °C of the sample processed to a single ECAP pass, down to

12

351 °C for the sample processed to twelve ECAP passes. This unknown peak found in the deformed material during all ECAP passes can be a presentation of the recrystallisation temperature as suggested by Vedani et al. [16] results.

4. Conclusion

AA6060 was SPD-processed by ECAP at room temperature through a die of an inner angle of Φ=90º from 1 to 12 passes. The XRD analysis has shown an ultra-fine grain structure with an average crystallite size than 45 nm in ECAPed samples. Relatively, the increase in the number of ECAP passes promotes a decrease at the level of the lattice parameter because of the partial dissolution of the precipitates. Regarding the EBSD analysis, it revealed that the microstructure of the sample after a single ECAP pass consists mainly of elongated grains, in the association with subgrain formation. An heterogeneous ultra-fine grain structure with an average grain sizes of 0.57 and 0.47 μm was obtained after 8 and 12 passes, respectively. The DSC analysis has proven a shift in peak positions and differences in shapes regarding the undeformed alloy. The peaks for metastable β'' and β' precipitates were anticipated. The creation of β stable phase was undergone some partial suppression in the alloy processed to 1 up 12 ECAP passes, probably because of the anticipated Si-rich particles precipitation.

References

1. Valiev RZ, Islamgaliev RK, Alexandrov IV (2000) Bulk nanostructured materials from severe plastic deformation. Prog Mater Sci 45:103-189.

2. Zehetbauer MJ, Zhu YT (2009) Bulk Nanostructured Materials.VCH Wiley, New York.

3. Valiev RZ, Zhilyaev AP, Langdon TG (2014) Bulk Nanostructured Materials: Fundamentals and Applications, TMS-Wiley, Hoboken, New Jersey.

4. Valiev RZ, Estrin Y, Horita Z, Langdon TG, Zehetbauer MJ, Zhu YT (2006) Producing bulk ultrafine-grained materials by severe plastic deformation. JOM 58:33-39.

5. Dalla Torre F, Lapovok R, Sandlin J, Thomson PF, Davies CHJ, Pereloma EV (2004) Microstructures and properties of copper processed by equal channel angular extrusion for 1-16 passes. Acta Mater 52: 4819-4832.

6. Ungar T, Borbely A (1996) The effect of dislocation contrast on x-ray line broadening: A new approach to line profile analysis. J Appl Phys Lett 69:3173- 3175.

7. Mhadhbi M, Khitouni M, Escoda L, Suñol JJ (2010) X-ray studies of structure defects in nanostructured FeAl alloy. Mater Lett 64:1802-1805.

8. Sort J, Nogués J, Suriñach S, Muñoz JS, Baró MD (2004) Correlation between stacking fault formation, allotropic phase transformations and magnetic properties of ball-milled cobalt. Mater Sci Eng A 375:869-873.

9. Huang JY, Wu YK, Ye HQ, Lu K (1995) Allotropic transformation of cobalt induced by ball milling. NanoStruct Mater 6:723-726.

10. Langford JI (1992) National Institute of Standards and Technology Special Publication 846 in: Proceedings of the International Conference Accuracy in Powder Diffraction II, NIST, Gaithersburg, MD.

11. Iwahashi Y, Horita Z, Nemoto M, Langdon T.G (1997) An investigation of microstructural evolution during equal-channel angular pressing. Acta Mater 45:4733-4741.

12. Ferrasse S, Segal VM, Hartwig KT, Goforth RE (1997) Microstructure and properties of copper and aluminum alloy 3003 heavily worked by equal channel angular extrusion. Metall Mater Trans A 28:1047-1057.

13. Panigrahi SK, Jayaganthan R, Pancholi V, Gupta M (2010) A DSC study on the precipitation kinetics of cryorolled Al 6063 alloy. Mater Chem Phys 122:188-193.

14. Yassar RS, Field DP, Weiland H (2005) The effect of cold deformation on the kinetics of the β'' precipitates in an Al-Mg-Si alloy. Metall Mater Trans A 36:2059-2065.

15. Fare S, Lecis N, Vedani M (2011) Aging Behaviour of Al-Mg-Si Alloys Subjected to Severe Plastic Deformation by ECAP and Cold Asymmetric Rolling. J Metallurgy 2011:1-8.

16. Vedani M, Angella G, Bassani P, Ripamonti D, Tuissi A (2007) DSC analysis of strengthening precipitates in ultrafine Al-Mg-Si alloys, JTherm Anal Calorim 87:277-284.

17. Iwahashi Y, Wang J, Horita Z, Nemoto M and Langdon TG (1996) Principle of equal-channel angular peessing for the processing of ultra-fine grained materials, Scr Mater 35:143-146.

18. Langford JI (1978) A rapid method for analysing the breadths of diffraction and spectral lines using the Voigt function. Appl Cryst 11:10-14.

19. Azàroff LV, Buerger M (1958) The powder Method, Mc Graw-Hill, New York, 238-245.

20. Griger A (1987) Powder Diffraction Data for the α H Intermetallic Phases with Slight Variation in Composition in the System Al-Fe-Si. Powder Diffr 2:31-35.

21. Korchef A, Njah N, Champion Y, Guérin S, Leroux C, Masmoudi J, Kolsi A (2004) Material flow during equal channel angular pressing of aluminum containing Al_8Fe_2Si precipitates. Adv Eng Mater 6:222-228.

22. Noda Y, Kon H, Furukawa Y, Otsuka N, Nishida I, Masumoto KA (1992) Preparation and Thermoelectric Properties of Mg_2Si_{1-x} Ge x (x=0.0∼ 0.4) Solid Solution Semiconductors Mater Trans (JIM) 33:845-850.

23. Yassar RS, Field DP, Weiland H (2005) The effect of cold deformation on the kinetics of the β ″precipitates in an Al-Mg-Si alloy. Metall Mater Trans A 36:2059-2065.

24. Rebhi A, Makhlouf T, Njah N, Champion Y, Couziniéb JP (2009) Characterization of aluminum processed by equal channel angular extrusion: Effect of processing route. Mater Charact 60:1489-1495.

25. Reyes-Ruiz C, Figueroa IA, Braham C, Cabrera JM, Alfonso I, Gonzalez G (2015) Texture and Lattice Distortion Study of an Al-6061-T6 Alloy Produced by ECAP. Mater Trans 56:1781-1786.

26. Swanson HE, Tatge E (1953) Standard X-ray diffraction powder patterns. Natl Bur Stand (US) Circ 5391:23-33.

27. Bletry A (1970) Effets de taille dans les solutions solides de l'aluminium avec les metaux de transition de la premiere serie. J Phys Chem Solids 3 :1263-1272.

28. Fuzayev AP, Tsenev EF (1950) Zh Tekh Fiz 20:66.

29. Gubicza J, Nam NH, Balogh L, Hellmig RJ, Stolyarov VV, Estrin Y, Ungár T (2004) Microstructure of severely deformed metals determined by X-ray peak profile analysis. J Alloys Compd 378:248-252.

30. Gubicza J, Chinh NQ, Krállics Gy, Schiller I, Ungár T (2006) Microstructure of ultrafine-grained fcc metals produced by severe plastic deformation. Curr App Phys 6:194-199. 32.

31. Korchef A, Njah N, Kolsi AW (2009) Microstructure investigation of equal channel angular pressed aluminium by X-ray diffraction and scanning electron microscopy. Cryst Res Technol 44:106 - 110.

32. Senthil Saravanan M S, Kumaresh Babu SP (2015) Synthesis, Characterization, and ECAP Consolidation of Carbon Nanotube Reinforced AA 4032 Nanocrystalline Composites Produced by High Energy Ball Milling. J Eng Mater Technol 137: 021004-021009.

33. Zhao YH, Shang HW, Lu K (2001) Microstructure evolution and thermal properties in nanocrystalline Fe during mechanical attrition. Acta Mater 49:365-375.

34. Horita Z. Xu C, Langdon T G (2011) Microstructural evolution in an aluminum solid solution alloy processed by ECAP. Mater Sc Eng A 528:6059-6065.

35. Kawasaki M, Horita Z, Langdon TG (2009) Microstructural evolution in high purity aluminum processed by ECAP. Mater Sci Eng A 524:143-150.

36. Kim WJ, Sa YK, Kim HK, Yoon US (2008) Plastic forming of the equal-channel angular pressing processed 6061 aluminum alloy. Mater Sci Eng A 487:360-368.

37. Iwahashi Y, Horita Z, Nemoto M, Langdon T G (1998) Factors influencing the equilibrium grain size in equal-channel angular pressing: Role of Mg additions to aluminum. Metall Mater Trans A 29:2503-2510.

38. Bay B, Hansen N, Hughes DA, Kuhlmann-Wilsdorf D (1992) evolution of f.c.c. deformation structures in polyslip. Acta Metal Mater 40:205-219.

39. Biroli G, Caglioti G, Martini L, Riontino G (1998) Precipitation kinetics of AA4032 and AA6082 A comparison based on DSC and TEM. Scr Mater 39:197-203.

17

40. Gupta K, Lloyd DJ, Court SA (2001) Precipitation hardening in Al–Mg–Si alloys with and without excess Si. Mater Sci Eng A 316:11-17.

41. Edwards GA, Stiller K, Dunlop GL, Couper MJ (1998) The precipitation sequence in Al–Mg–Si alloys. Acta Mater 46:3893-3904.

42. Matsuda K, Sakaguchi Y, Miyata Y, Uetani Y, Sato T, Kamio A, Ikeno S (2000) Precipitation sequence of various kinds of metastable phases in Al-1.0wt% Mg_2Si-0.4 wt% Si alloy. J Mater Sci 35:179 -189.

Figures captions:

Fig. 1 Schematic illustration showing the geometry of the ECAP die.

Fig. 2 X-ray diffraction patterns of AA6060 alloy before (0 Passes) and after ECAP (1 Pass

to 12 Passes).

Fig. 3 Profile of the (111) peak and (200) peak Bragg reflections as a function of the number

of passes.

Fig. 4 Halder-Wagner plots for the AA6060 at different ECAP passes.

Fig. 5 Evolutions of the crystallite sizes and the lattice strains as a function of the number of

passes.

Fig. 6 Variation of lattice strain and theoretical strain introduced by ECAP process as a
function of number of passes.

Fig. 7 Evolution of lattice parameter for AA6060 as a function of number of passes.

Fig. 8 Evolution of the dislocation density, ρ as a function of number of passes.

Fig. 9 Band contrast maps with LAGB ($3° \leq \theta \leq 15°$) in white and HAGBs ($\theta > 15°$) in black

lines of AA6060 (a) 0 pass, after (b) 1 pass, (c) 2passes, (d) 3 passes,(e) 4 passes,

(f) 5 passes , (g) 6 passes , (h) 8 passes and (e) 12 passes .

Fig. 10 Histograms of the misorientation angles in AA6060 (a) 1, (b) 2, (c) 4, (d) 5, (e) 8 and

(f) 12 passes of ECAP.

Fig. 11 Dependence of the (a) grain size and (b) the amount of HAGB and LAGB on the

number of ECAP passes.

Fig. 12 DSC curves of the Al–Mg–Si alloy as a function of ECAP passes (heating rate 20°C

min^{-1}).

Fig. 13 Dependence of the peak β'on the number of ECAP passes.

Tables captions:

Table 1 Chemical composition of aluminum alloy (AA6060) wt.%

19
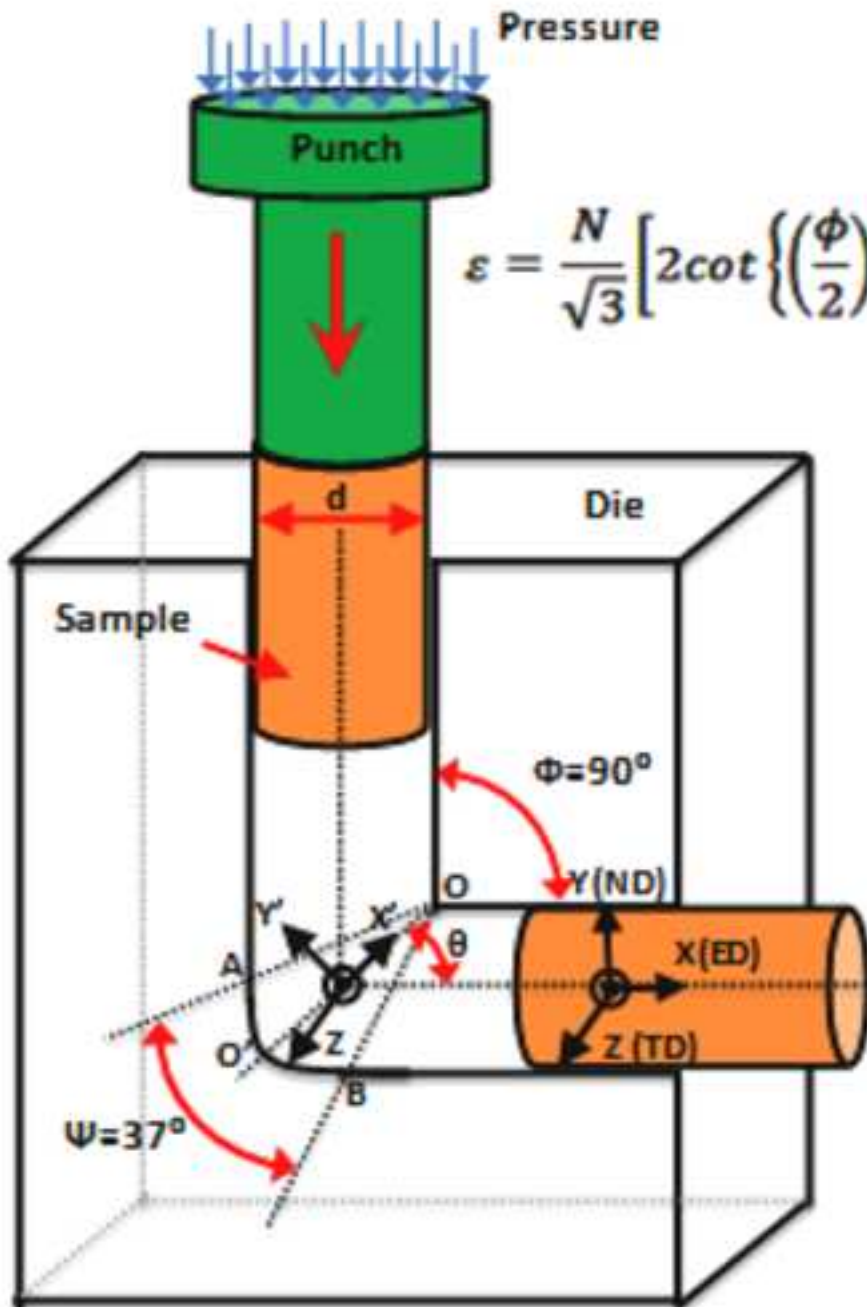
$$\varepsilon = \frac{N}{\sqrt{3}}\left[2\cot\left\{\left(\frac{\phi}{2}\right)+\left(\frac{\psi}{2}\right)\right\}+\psi\,cosec\left\{\left(\frac{\phi}{2}\right)+\left(\frac{\psi}{2}\right)\right\}\right]$$

- Bars: 10mm diameter; 60mm length
- Ram speed: 20mm/s
- Lubricant: MoS_2
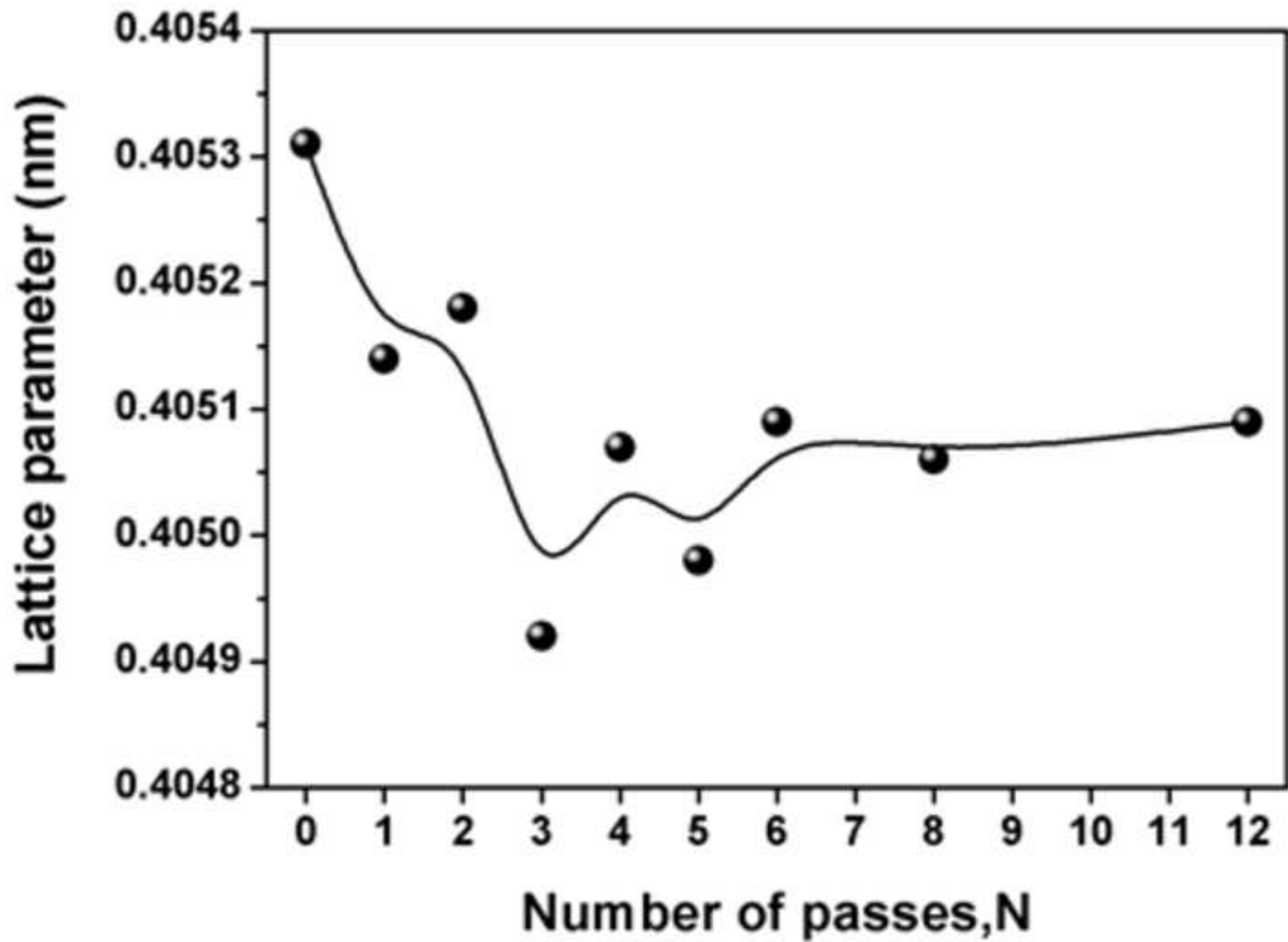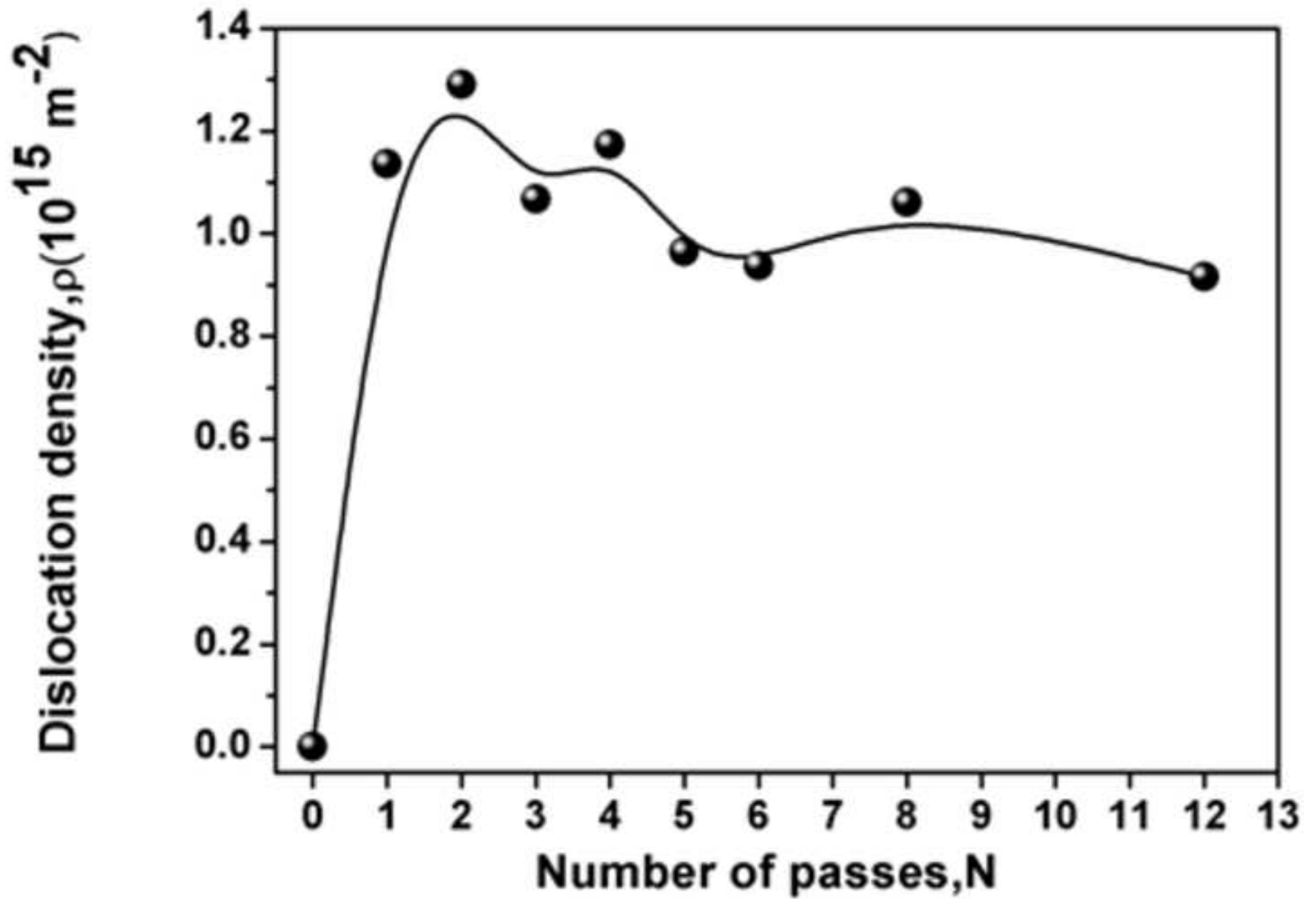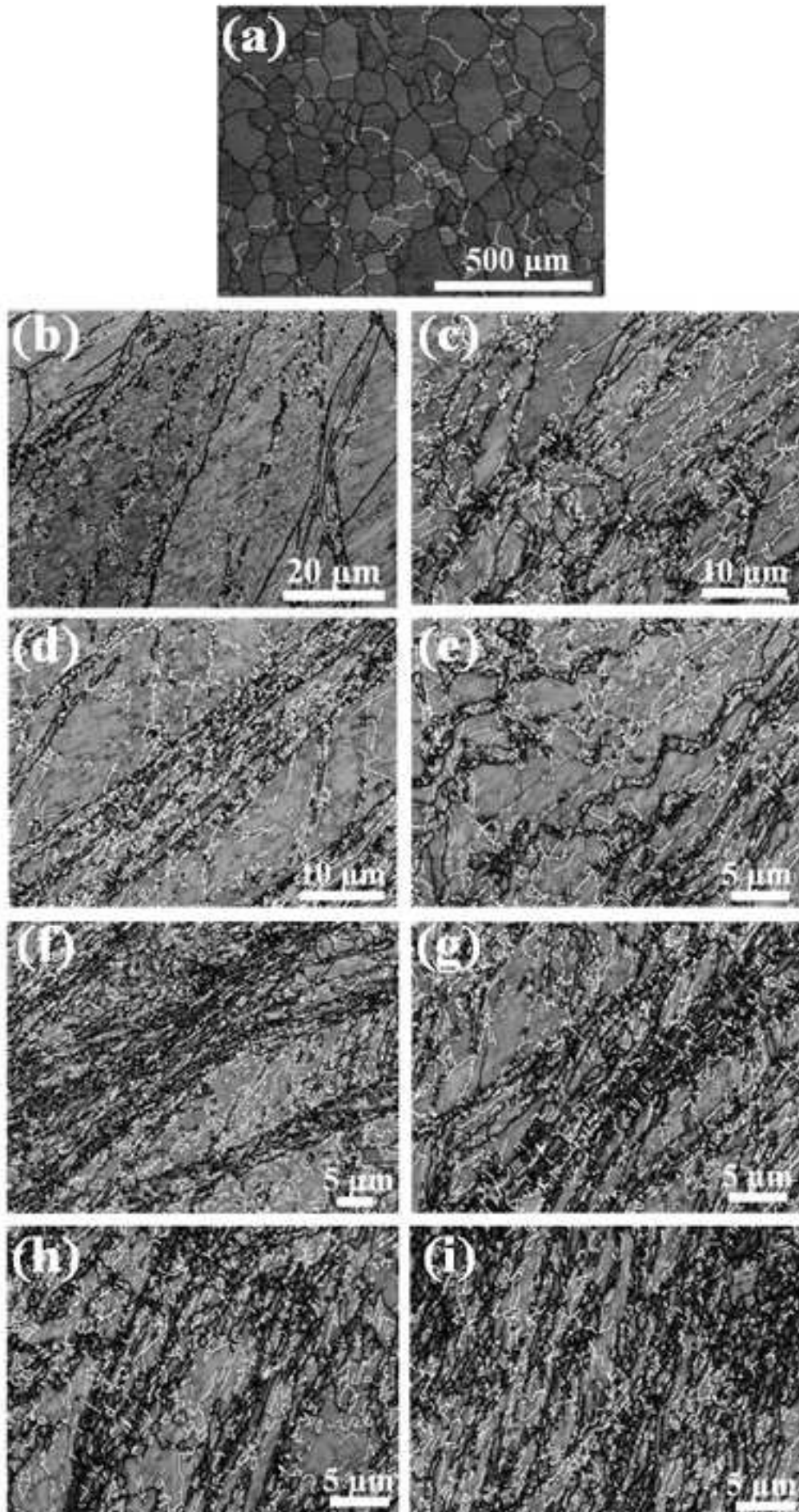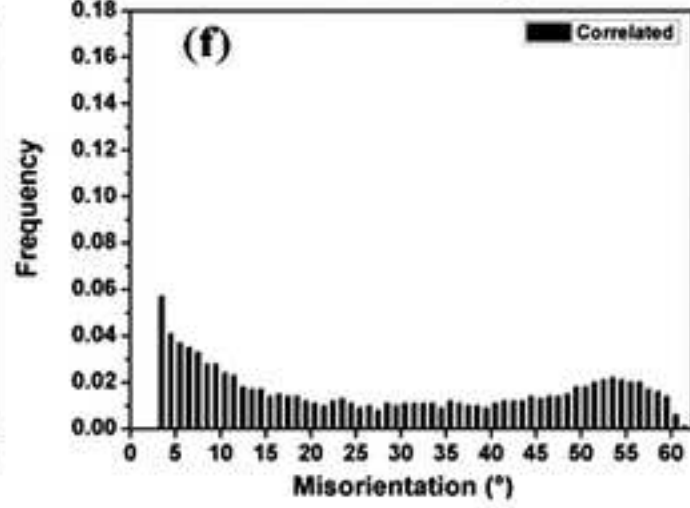- 12 passes
- Room temperature
- $\Phi = 90°$; $\psi = 37°$
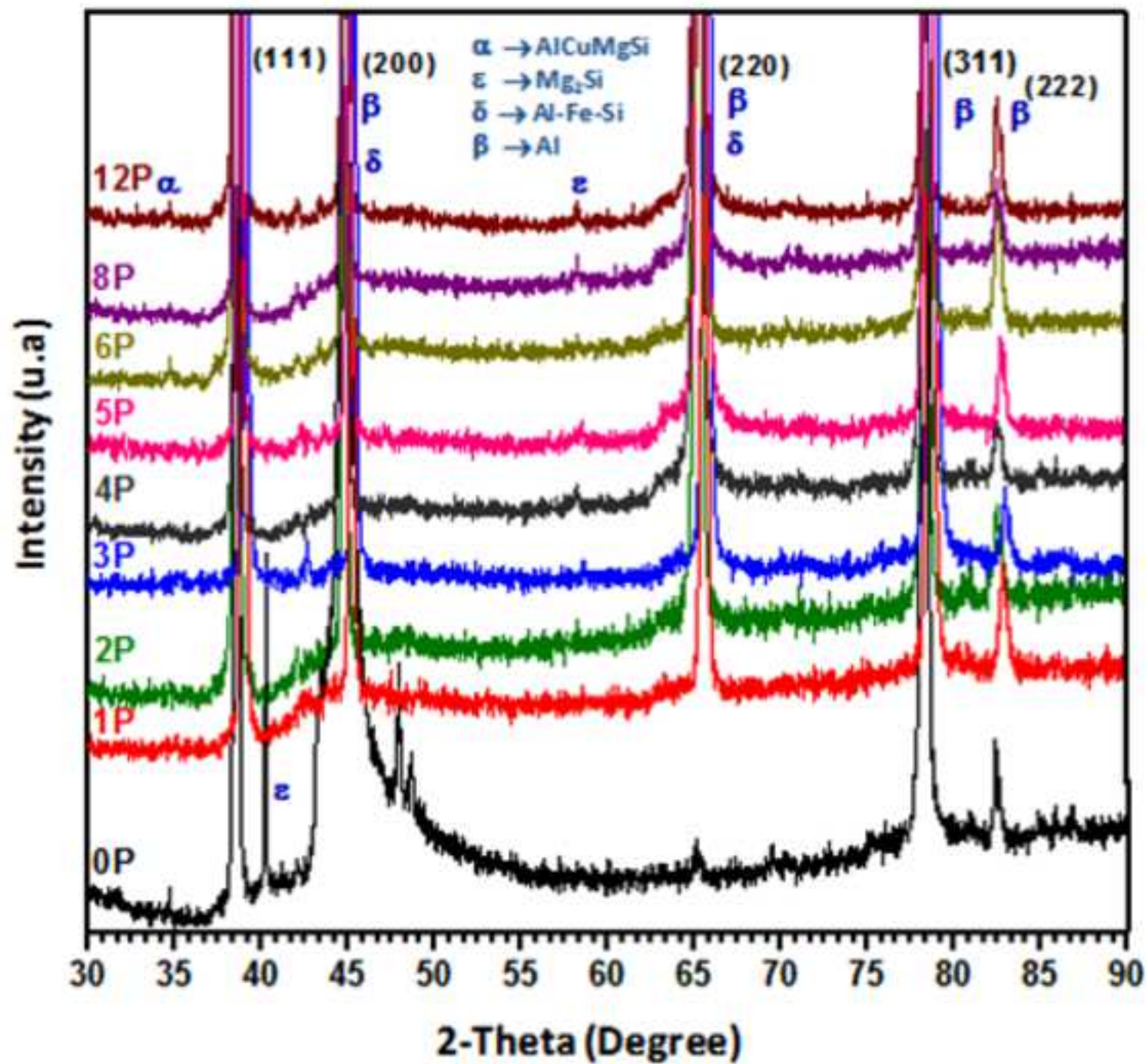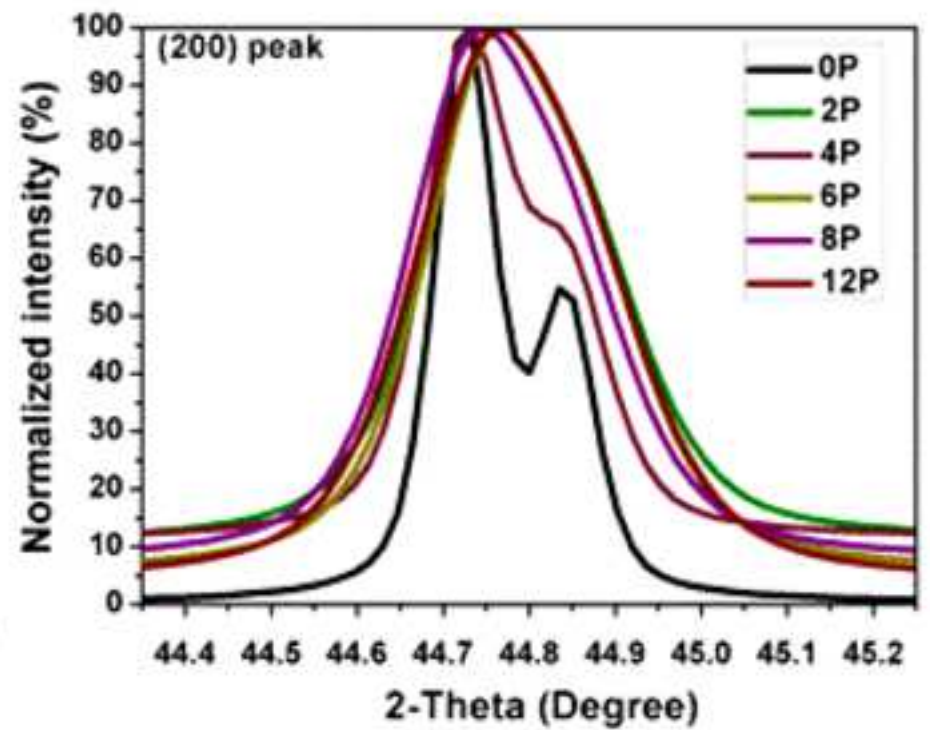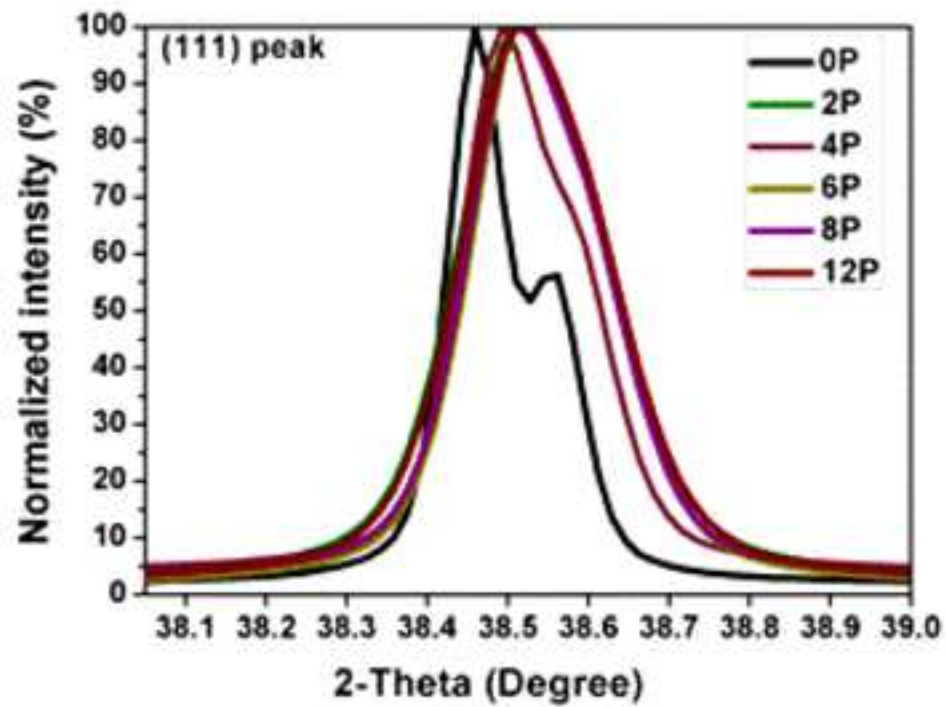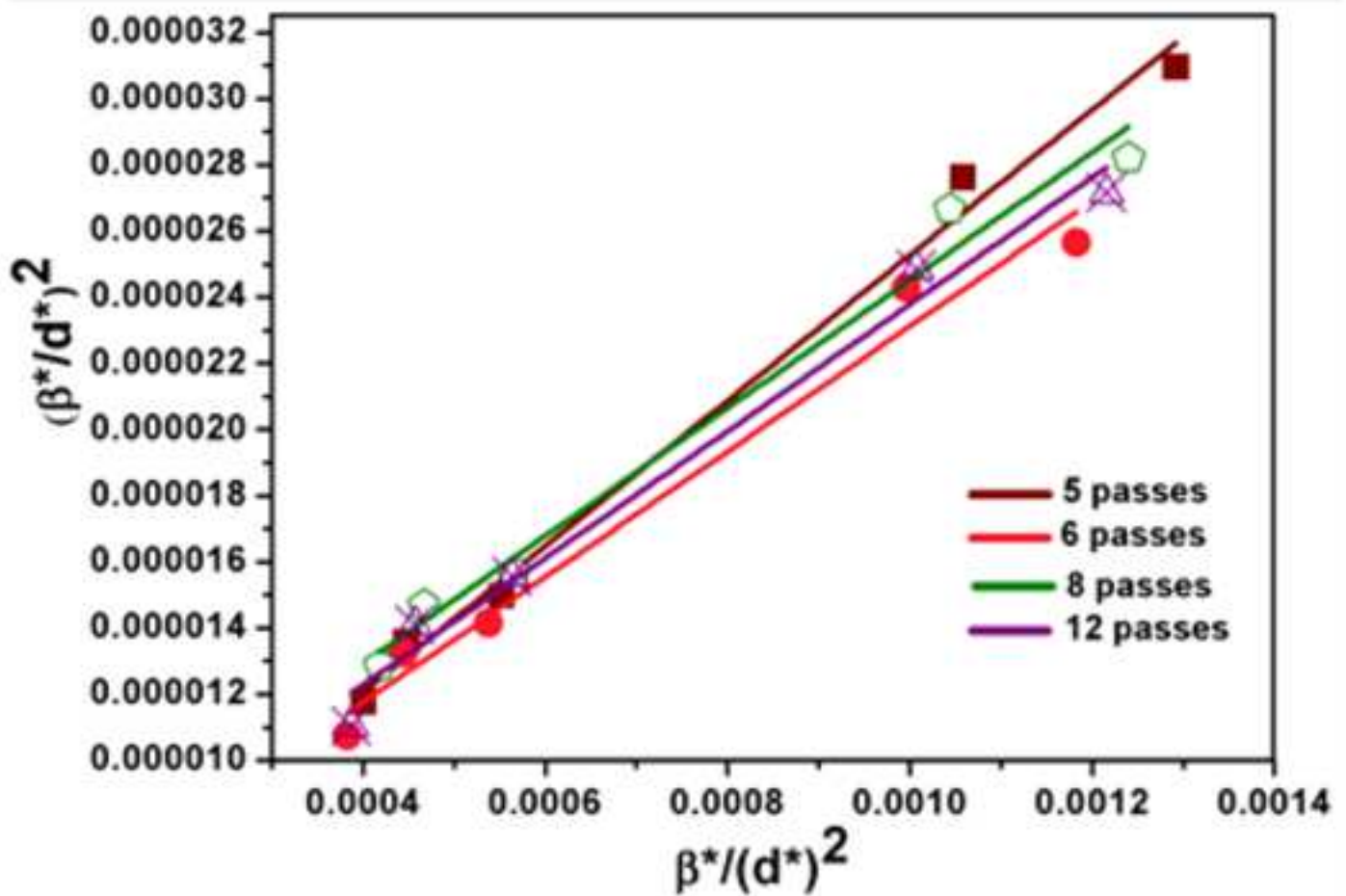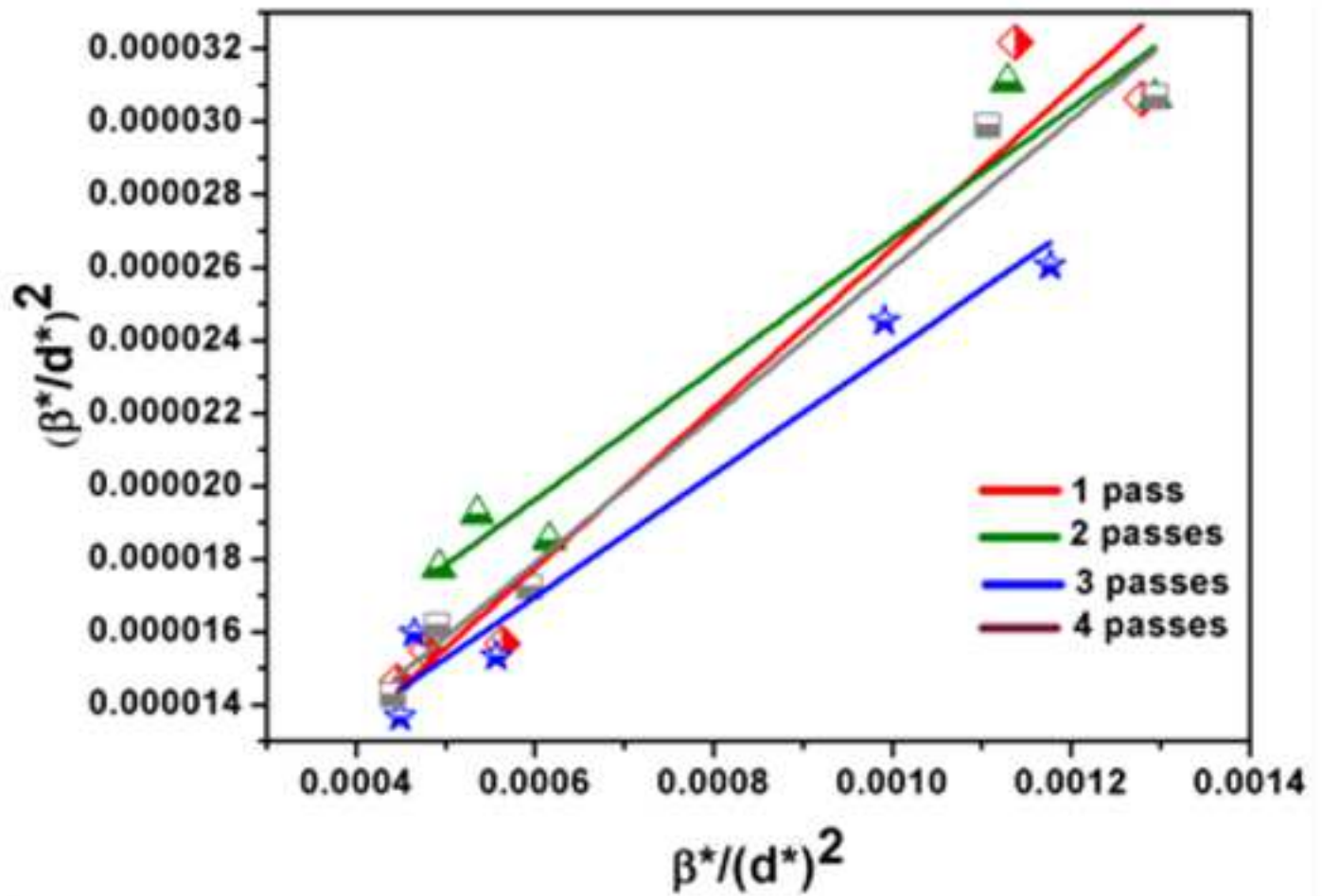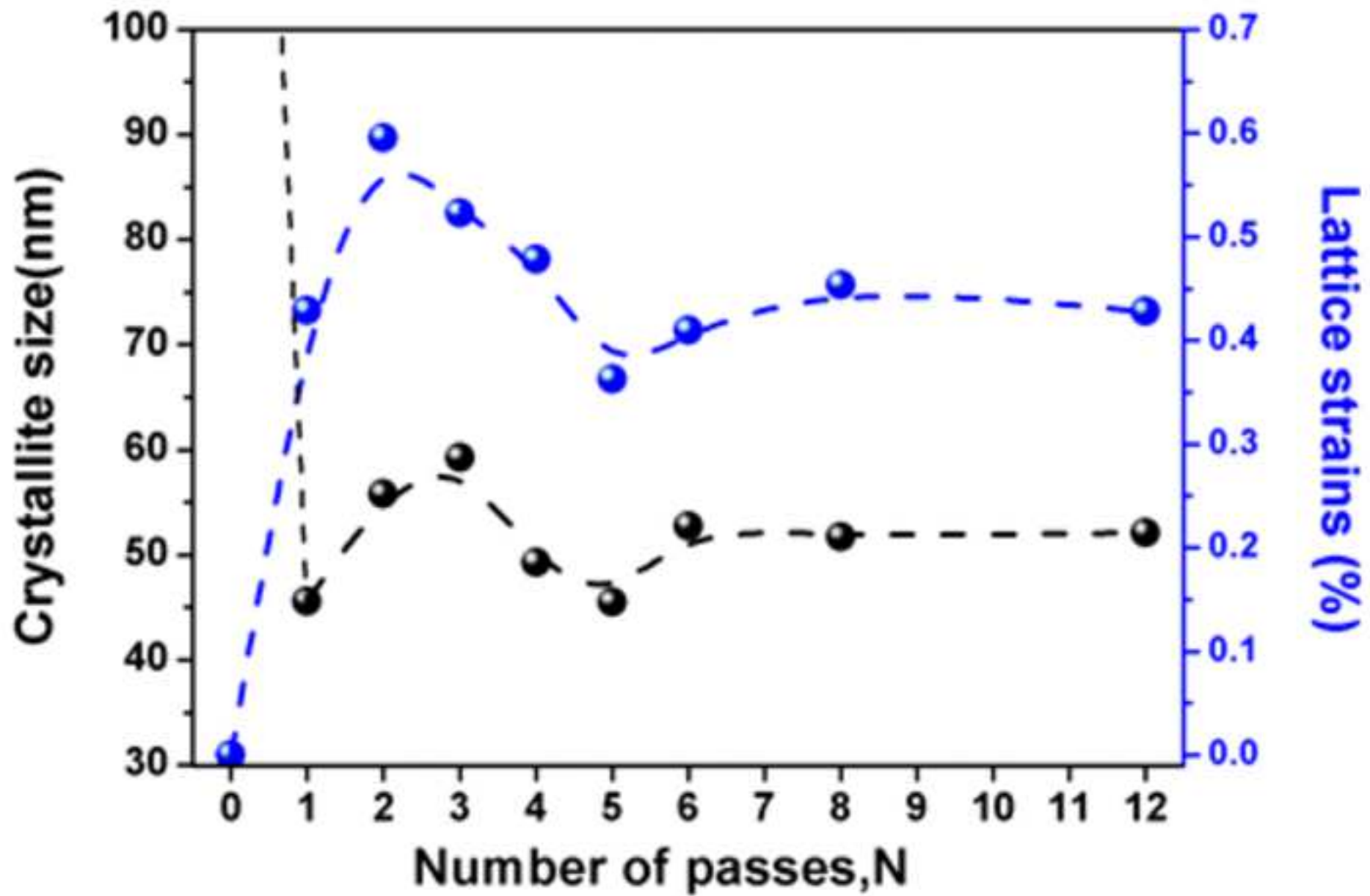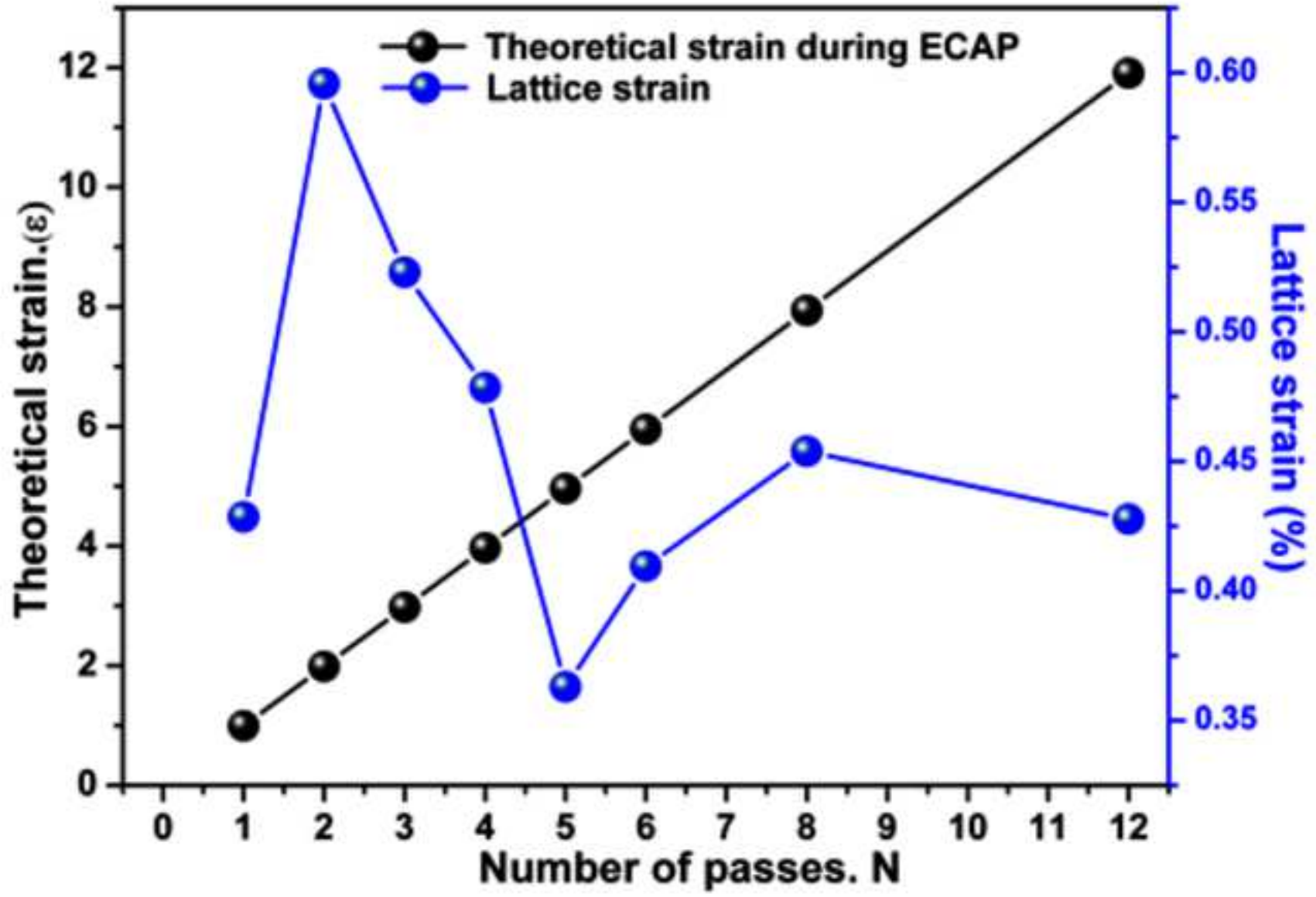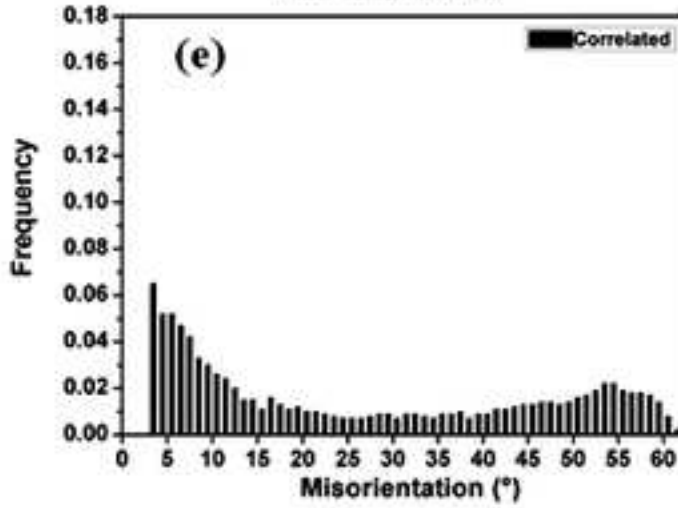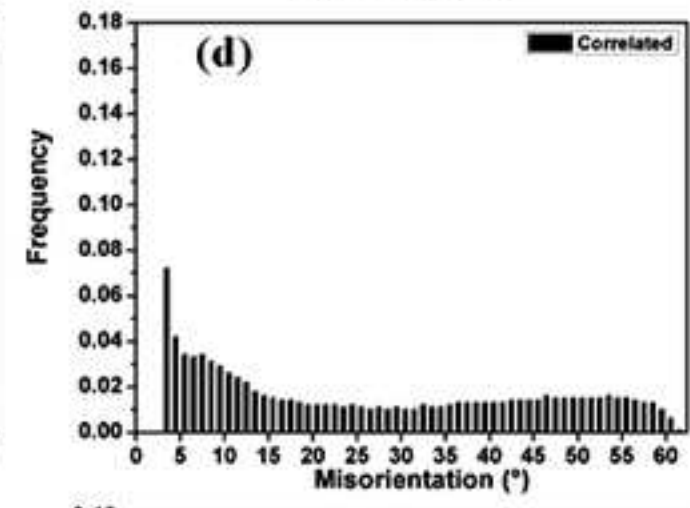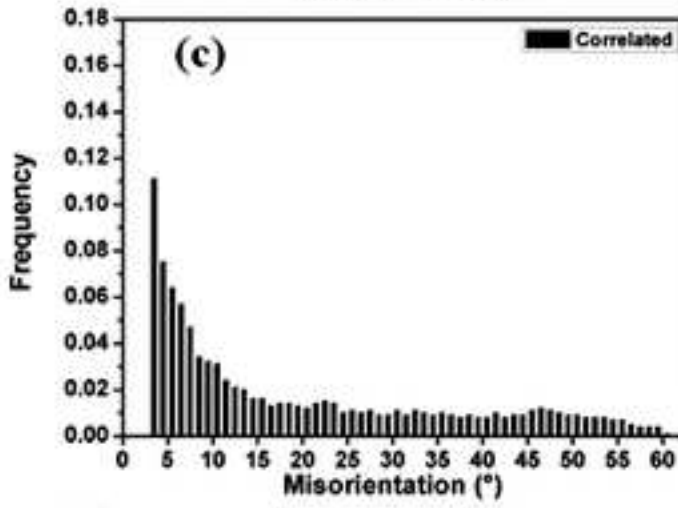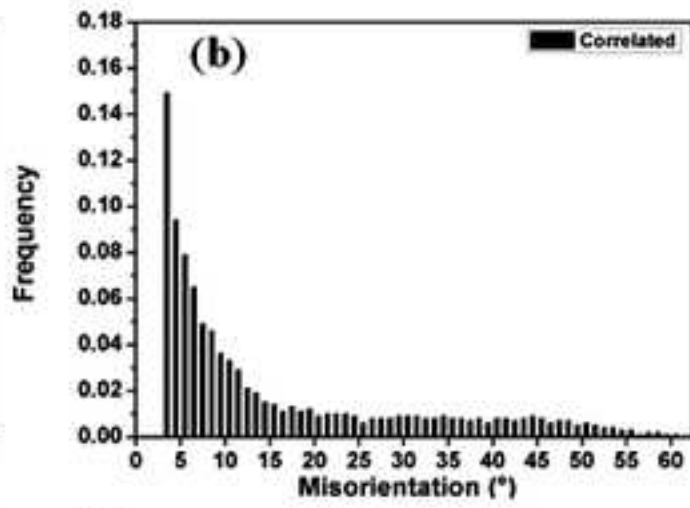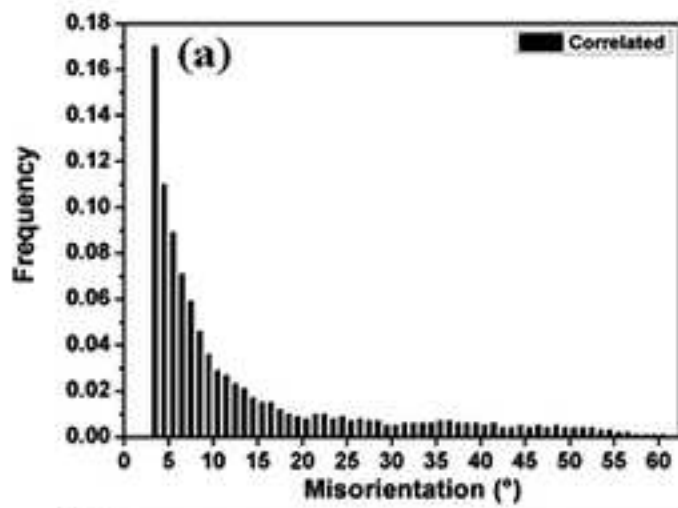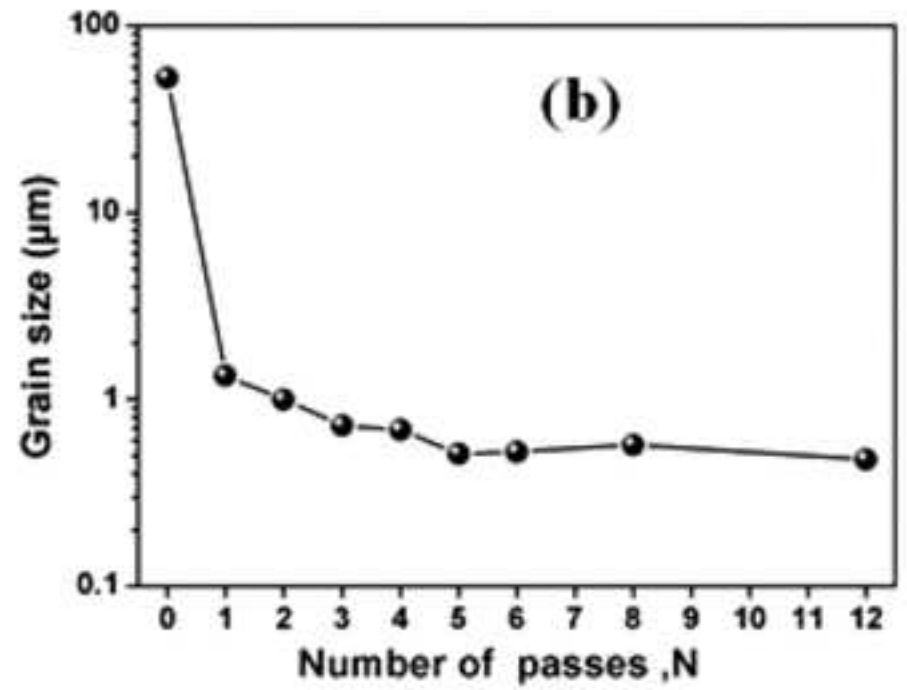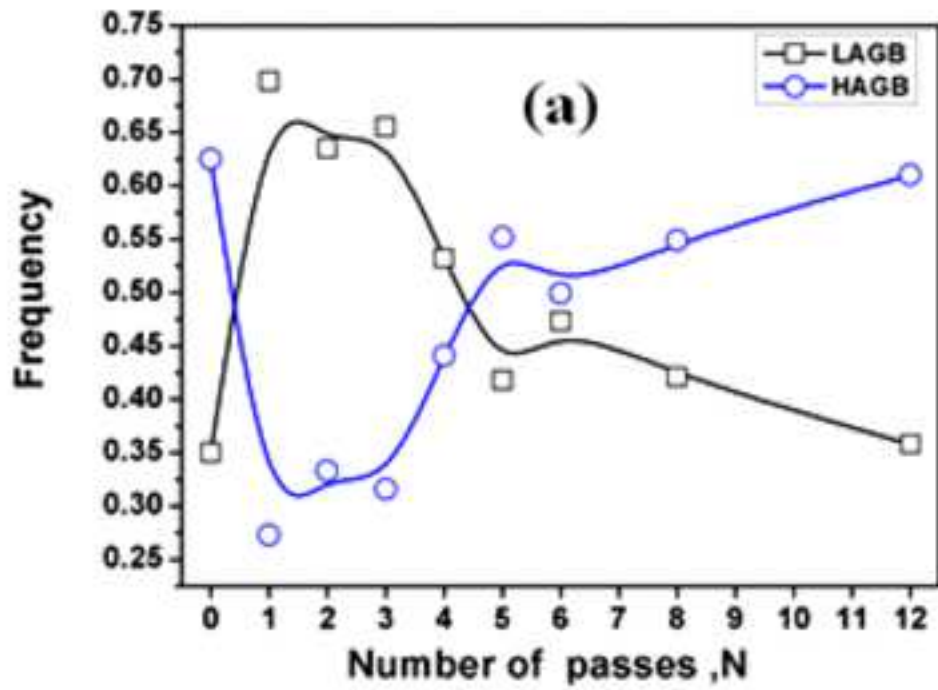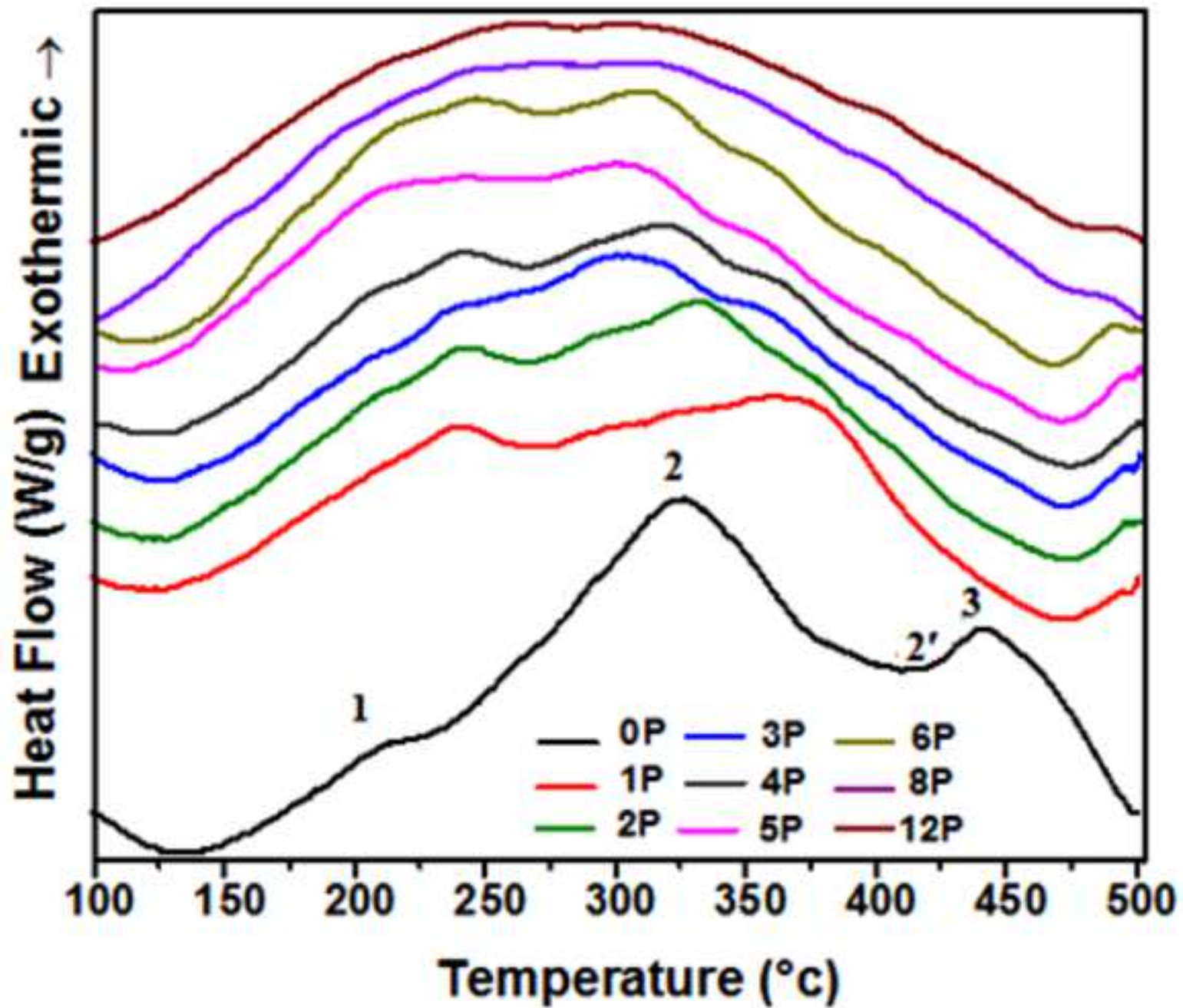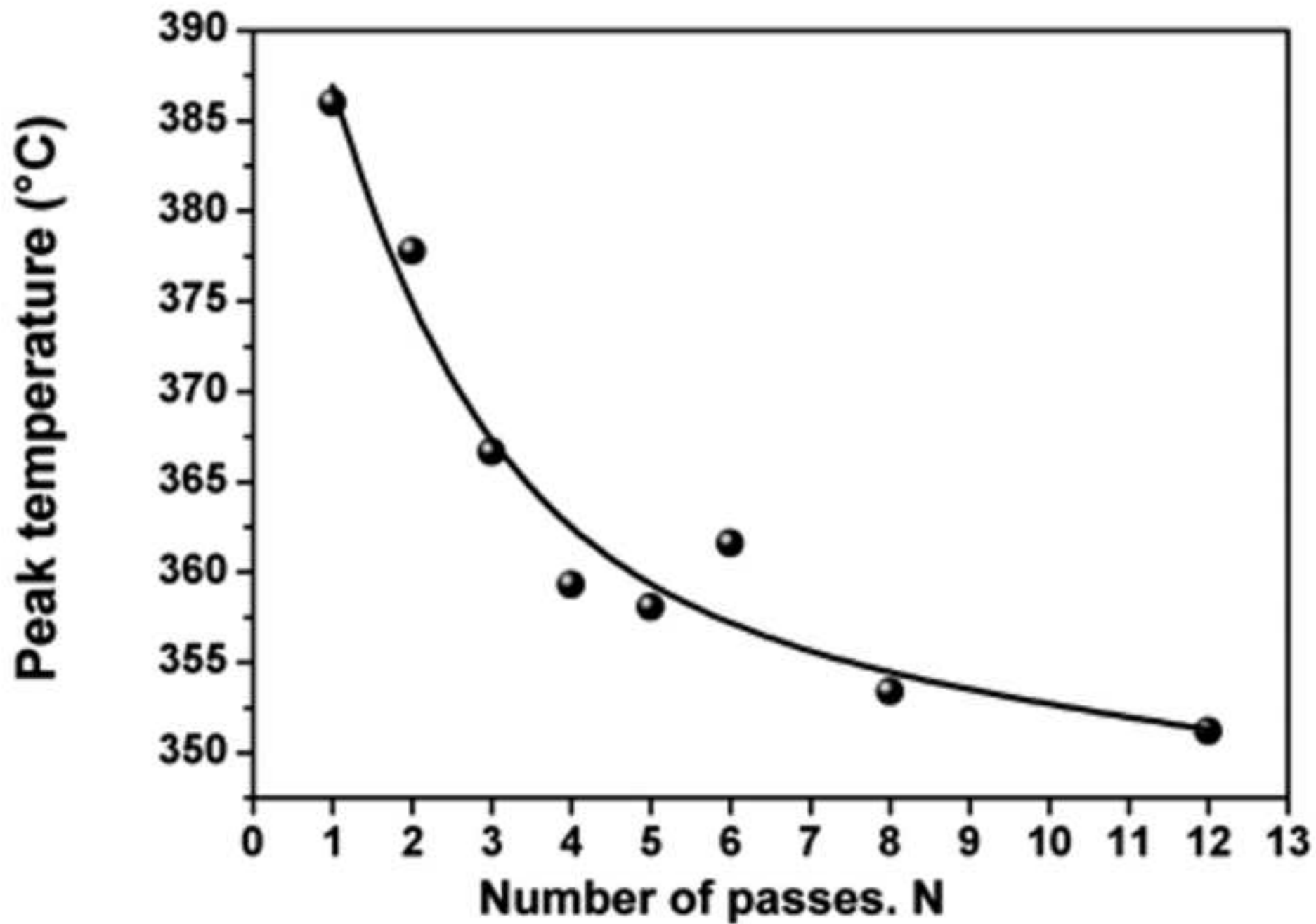
Table.1

Element	wt.%	Element	wt.%	Element	wt.%
Al	98.76	Ca	0.0004	Zn	0.002
V	0.008	Ti	0.011	Mg	0.454
Sr	0.0002	Sn	0.002	Mn	0.024
Sb	0.0773	Pb	0.004	Cu	0.001
P	0.0010	Cr	0.001	Fe	0.205
Na	0.0008	Ni	0.001	Si	0.449